Electronic bands and optical conductivity of the Dzyaloshinsky-Moriya multiferroic $Ba_2CuGe_2O_7$

M. Corasaniti,[1] P. Barone,[2] A. Nucara,[3] M. Ortolani,[1] L. Baldassarre,[3] R. Fittipaldi,[4] V. Granata,[4] L. Rocco,[4] A. Vecchione,[4] W. S. Mohamed,[5] J. Lorenzana,[6] and P. Calvani[3]

[1]*Dipartimento di Fisica, Sapienza Università di Roma, P.le A. Moro 5, 00185 Roma, Italy*

[2]*CNR-SPIN c/o Università dell'Aquila, L'Aquila, Italy*

[3]*CNR-SPIN and Dipartimento di Fisica, Sapienza Università di Roma, P.le A. Moro 5, 00185 Roma, Italy*

[4]*CNR-SPIN and Dipartimento di Fisica "E. R. Caianiello", Via Ponte don Mellillo, I-84084 Fisciano, Salerno, Italy*

[5]*Physics Department, Faculty of Science, Sohag University, 82524 Sohag, Egypt*

[6]*CNR-ISC c/o Dipartimento di Fisica, Sapienza Università di Roma, P.le A. Moro 5, 00185 Roma, Italy*

(Received 31 January 2017; revised manuscript received 2 July 2017; published 10 August 2017)

We have measured the reflectivity in the *ab* plane and along the *c* axis of a single crystal of the Dzyaloshinsky-Moriya multiferroic $Ba_2CuGe_2O_7$, from 20 to 300 K and from 700 to 24 000 cm^{-1}. The resulting optical conductivity $\sigma(\omega)$ has been compared with the results of calculations of its electronic band structure based on density functional theory (DFT). A broad midinfrared band, which in the *ab* plane strongly hardens for decreasing temperature, is consistent with d-d transitions of the Cu atom. A further electronic absorption, whose edge falls in the near infrared and has a strong O-*p* character, unusually softens with decreasing temperature by more than 0.15 eV, in both polarizations. Calculations show that the behavior with temperature of those electronic bands can be related to distortions of the CuO_4 tetrahedra.

DOI: 10.1103/PhysRevB.96.085115

I. INTRODUCTION

Magnetoelectric (ME) materials belong to a class of multiferroics where the magnetization can be controlled by an electric field or, inversely, the electric polarization can be switched on by a magnetic field. The growing interest for these compounds, most of which are oxides, is partly justified by their intrinsic physical interest, partly by the perspective of implementing a new generation of microelectronic devices [1]. Therefore, several potentially ME materials have been explored in the last two decades. Among them one should mention those which exploit charge/spin ordering, like $LuFe_2O_4$ [2,3], and those based on the Dzyaloshinsky-Moriya (D-M) spin exchange [4,5]. For example, the room-temperature magnetoelectricity [6] of $BiFeO_3$ has been recently explained in terms of D-M interactions which both produce its helical magnetic ordering and are able to induce an electric dipole moment [7,8]. Another interesting D-M material is $Ba_2CuGe_2O_7$ (BCGO), whose noncentrosymmetric, tetragonal structure ($P\bar{4}2_1m$) includes corner-shared CuO_4 and GeO_4 tetrahedra. The *c* axis of the cell is shorter (0.5445 nm) than the *a*,*b* axes (0.8466 nm). BCGO develops helical magnetism below $T_N = 3.2$ K through a D-M spin coupling [9–14] with the formation of two opposite magnetic domains [13], which can be easily aligned with each other by applying a weak magnetic field in the *ab* plane. The D-M effect characterizes BCGO with respect to isostructural magnetoelectric compounds like $Ba_2MnGe_2O_7$, $Ba_2CoGe_2O_7$, and $Sr_2FeGe_2O_7$, which present an antiferromagnetic (AF) ground state [15–18].

Up to now, the optical properties of this important family of multiferroics were studied in the terahertz (THz) and far-infrared region. The infrared phonons of $Ba_2CoGe_2O_7$ were investigated in association with neutron scattering [19] while, in the same compound, electromagnon excitations were detected by THz time-domain spectroscopy [20]. This technique was also applied to $Sr_2FeGe_2O_7$ to point out the effect of Fe-O tetrahedra compression on spin-orbit coupling [18]. For $Ba_2CuGe_2O_7$, we presented far-infrared [21] and Raman [22] spectra which, together with shell-model calculations, demonstrated a strong electron-phonon coupling in this compound at low temperature. In the present paper we extend our study of BCGO to the electronic bands by presenting optical spectra taken at different temperatures from 700 to 24 000 cm^{-1} with the radiation polarized in the *ab* plane and along the *c* axis. Indeed, determining the electronic structure of a new material, and especially of its optical gap, is important in itself and in view of its potential applications. The experimental optical conductivity $\sigma(\omega)$ was then compared with that extracted from band calculations based on density functional theory. The theoretical $\sigma(\omega)$ was found to be very sensitive to the distortion of the CuO_4 tetrahedra of the BCGO structure, which may qualitatively explain the strong and unusual temperature dependence of the electronic bands pointed out by the present measurements.

II. EXPERIMENT AND RESULTS

Single crystals of BCGO were grown, like those prepared for our previous experiments [21,22], by the optical floating-zone melting method [23]. They were then characterized by high resolution x-ray diffraction and scanning electron microscopy combined with energy dispersive spectroscopy at room temperature. The crystal orientation was determined by x-ray back-reflection Laue method [23]. The *ac* (or *bc*) surface was finely polished with powders down to 0.3 μm in grain size. As the crystals are nearly transparent in the whole spectral region of interest, to avoid interference fringes their back surface was left unpolished and was wedged with respect to the front surface. The sample was mounted on the cold finger of a helium-flow cryostat together with a gold mirror which served as reference in the midinfrared (replaced by an aluminum mirror for the near infrared and the visible) that was aligned parallel to the sample surface with a laser beam. The sample reflectivity $R(\omega)$ was measured from 600 to 12 000 cm^{-1} by a

Michelson interferometer with a mercury-cadmium-tellerium detector, and from 10 000 to 24 000 cm^{-1} by a monochromator and a charge coupled device detector, with the radiation field polarized either along the a (b) axis or along the c axis. Further on, the former polarization will be indicated as lying in the ab plane. In the frequency intervals common to different spectral ranges, including that spanned in Ref. [21] (far infrared), $R(\omega)$ matched within 1%. The real part $\sigma(\omega)$ of the optical conductivity was then extracted from $R(\omega)$ by standard Kramers-Kronig transformations. At $\omega < 600$ cm^{-1} we used the above far infrared data and we extrapolated the reflectivity for $\omega \to \infty$ by assuming $R(\omega) \propto \omega^{-p}$, with $p = 2$ between 24 000 and 45 000 cm^{-1} and $p = 4$ elsewhere [24]. We judged that we obtained reliable results for $\sigma(\omega)$ up to $\omega \simeq$ 15 000 cm^{-1}.

The reflectivity of $Ba_2CuGe_2O_7$ is shown at different temperatures, for both polarizations, in Fig. 1. Therein one may remark the low absolute values of $R(\omega)$, which overcomes 0.2 in the visible range only. This is due to a sharp increase of the reflectivity, better shown in the insets, which at room temperature is observed around 13 000 cm^{-1} in the ab plane (a), around 14 000 cm^{-1} along the c axis (b). Both insets also show the temperature dependence of the edge of that absorption band in the near infrared (NIR), that we call NIR band, which unusually softens for decreasing temperature. In the main figure, both spectra also exhibit a band in the midinfrared (MIR) between about 2000 and 4000 cm^{-1} that we call the MIR band. It also exhibits a strong temperature dependence, but in the opposite way. The features around 1500 cm^{-1} in both panels, enhanced by the overall low reflectivity of the sample, may be tentatively ascribed to overtones of the highest-frequency strong phonons of BCGO.

The real part $\sigma(\omega)$ of the optical conductivity is shown in Fig. 2 for the whole spectral region of the present experiment. The narrow peaks in the far infrared are due to the highest-frequency phonon modes. Full infrared phonon spectra were already reported for both polarizations in Ref. [21] and will not be again discussed here. In Fig. 2, the lowest-energy broad feature is the above mentioned MIR band, which in the ab plane hardens between 300 and 20 K by more than 1000 cm^{-1}. On the contrary, the corresponding band measured along the

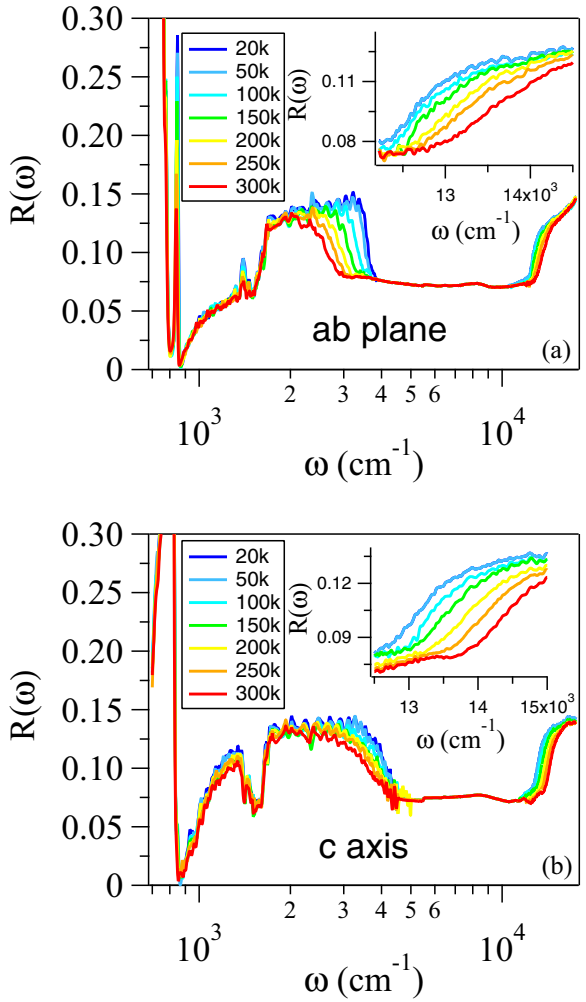

FIG. 1. Reflectivity of $Ba_2CuGe_2O_7$ from the far infrared to the visible, with the radiation polarized in the ab plane (a) and along the c axis (b), at different temperatures. In the insets, the spectral region of the near infrared is enlarged to highlight the temperature dependence of the highest-energy band edge.

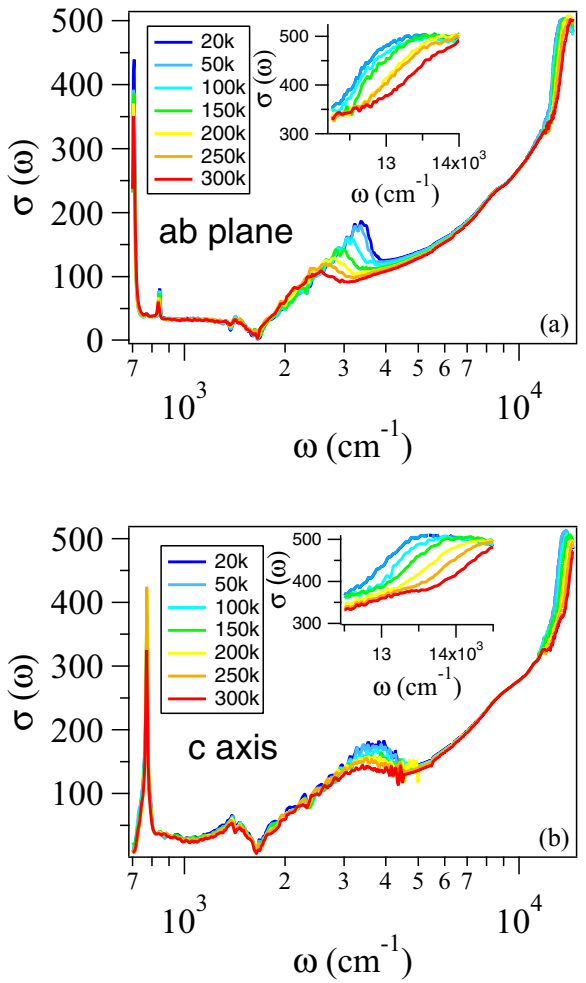

FIG. 2. Optical conductivity of $Ba_2CuGe_2O_7$ from the far infrared to the visible spectral region, with the radiation polarized along the a axis (a) and along the c axis (b), from 300 K to 10 K. In the insets, the spectral region of the near infrared is enlarged to better show the temperature dependence of the highest-energy band edge.

c axis does not shift appreciably, while its intensity grows smoothly for decreasing temperature. The already mentioned behavior with temperature of the edge of the nearinfrared (NIR) band, in both polarizations, is confirmed in Fig. 2. When cooling the sample from 300 to 20 K, it softens by about 1500 cm^{-1} in the ab plane, by even 2000 cm^{-1} along the c axis. As already remarked, this behavior is unusual, if compared for example with that of the optical gap in most semiconductors [25]. Also in cuprates, most of which have CuO_6 octahedra that are the counterpart of the present CuO_4 tetrahedra, the optical gap E_g of the Cu-O planes hardens for $T \to 0$. In the whole cuprate class [26], as well as in a cobaltate like [27] Na_xCoO_2, the charge-transfer gap shifts with the contraction of the Cu(Co)-O bond length d according to $E_g \propto d^{-7}$.

III. CALCULATION OF THE ELECTRONIC BANDS AND OF THE OPTICAL CONDUCTIVITY

A. Structural and computational details

Calculations based on density functional theory (DFT) have been performed in order to shed light on the origin of the MIR feature and to provide a qualitative understanding of the peculiar temperature dependence of both the MIR and NIR edges, showing opposite energy shifts when cooling. We performed DFT calculations using the projector-augmented waves (PAW) method as implemented in VASP [28] within the generalized-gradient approximation revised for solids (PBEsol) [29], except when specified. We used a $6 \times 6 \times 6$ Monkhorst-Pack k-points mesh and a 500 eV plane-wave cutoff for structural optimizations and a denser $14 \times 14 \times 14$ k-point mesh for band-structure calculations. Since the nonmagnetic phase always happens to be metallic, we imposed a C-type antiferromagnetic (AFM-C) configuration of Cu magnetic moments, i.e., ferromagnetic chains of spins along the tetragonal c axis antiferromagnetically coupled along the a and b directions. Indeed, the use of a broken symmetry solution to describe a system without broken symmetries is not an unusual approach in DFT [30]. We verified that the AFM-C pattern is the most stable collinear configuration of spins, happening to be the closest to the true low-temperature magnetic ground state. Indeed, the latter can be regarded as a modulation of the AFM-C state induced by relativistic Dzyaloshinskii-Moriya interaction, resulting in a transverse helical configuration comprising spin cycloids which propagate along the [110] direction and ferromagnetically coupled along the c axis.

Let us notice that the noncollinear magnetic phase develops at temperatures much smaller than the lowest temperature in the present experiment, and its accurate description—which would require large simulation supercells or even more sophisticated DFT schemes for dealing with noncollinear magnetism [31,32]—is beyond the scope of the present work, since we are mostly interested in the optical properties. One can object that in a strongly correlated system the optical absorption can depend on the spin configuration [33]. However, this dependence is due to intersite processes while in the present system we estimate that a large part of the spectral weight is due to transitions within a single tetrahedron, not affected by the spin-spin correlation. If the fraction of spectral weight due to intersite process may be overestimated in our computation, this is not so much due to the assumed spin-spin correlations, but because conventional DFT methods tend to underestimate Mott localization effects [34].

Also for the sake of simplicity, we did not allow the spins to relax in the presence of spin-orbit coupling (SOC). This is important in the Dzyaloshinskii-Moriya interaction which, however, would not be effective at the temperatures of the experiment. Nevertheless, we checked how spin-orbit coupling affects the electronic properties of BCGO and its related optical response by performing non-self-consistent calculations including SOC perturbatively with fixed collinear magnetic configuration.

Structural optimization has been performed starting from two different experimental structures, both showing $P\bar{4}2_1m$ tetragonal symmetry and lattice parameters $a = b = 8.466$ Å and $c = 5.445$ Å [35,36]. The most significant difference between the two experimental structures is the deformation of CuO_4 tetrahedra, which are found to be substantially undistorted in Ref. [35], while a strong Jahn-Teller compression

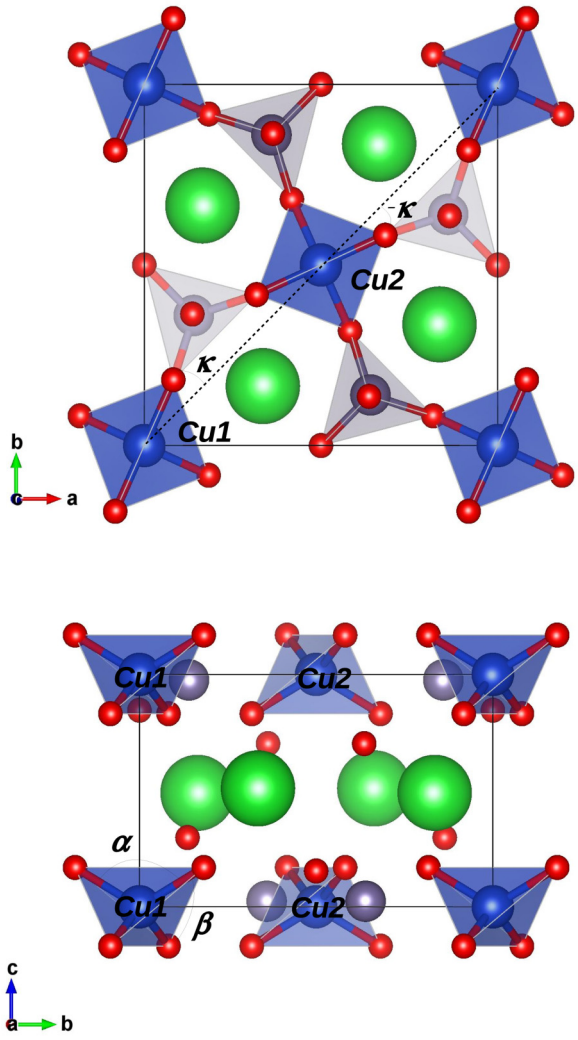

FIG. 3. Top (upper panel) and lateral (lower panel) view of the optimized structure, as obtained by imposing a C-type AFM structure (where the inequivalent Cu spins are opposite). The tilting angle κ and the tetragonal distortion defined by the O-Cu-O angles α and β are shown.

TABLE I. BCGO Experimental and calculated structural parameters: lattice constants $a(=b)$,c and c/a ratio; CuO_4 tilting angle κ about the c axis measured with respect to [110] direction; Cu-O bond length $l_{\text{Cu-O}}$ (Å) and O_{up}-Cu-$O_{up(lo)}$ bond angles α (β) (the subscript denoting upper- and lower-lying oxygens in each CuO_4 tetrahedron). Results obtained within the PBEsol functional are compared with those obtained with GGA Perdew-Burke-Enzerhof functional [40] and PBEsol + U [41] with $U = 4$ eV for Cu-d states.

	a (Å)	c (Å)	c/a	κ(°)	$l_{\text{Cu-O}}$ (Å)	α(°)	β(°)
Exp I [35]	8.466	5.445	0.643	19.8	1.89	108.7	109.9
Exp II [36]	8.466	5.445	0.643	20.1	1.94	123.4	103.0
GGA	8.628	5.548	0.643	20.8	1.97	123.7	102.9
PBEsol	8.506	5.472	0.643	20.7	1.94	124.0	102.7
PBEsol+U	8.477	5.480	0.646	20.6	1.93	122.0	103.6

along the tetragonal c axis has been reported in Ref. [36]. The amount of such distortion can be parametrized by the O-Cu-O bond angles α, between upper-lying oxygens in each tetrahedron, and β, which measures the O-Cu-O angle between upper- and lower-lying oxygens (see Fig. 3). To determine the optimal theoretical crystal structure, we fully relaxed both the lattice constants and atomic positions with different functionals usually adopted in solid-state physics, whose results are listed in Table I. All functionals provided consistent and comparable structural parameters, PBEsol functional showing the best agreement with the measured lattice parameters and c/a ratio. Our numerical simulations confirm the presence of highly distorted CuO_4 tetrahedra, in good agreement with the experimental data of Ref. [36]. Other more sophisticated functionals have been recently developed, such as the SG GGA and WC GGA functionals [37–39], which may improve the description of structural properties. Let us notice, however, that the strong local distortion of CuO_4 tetrahedra is always found in our calculations regardless of the DFT scheme, indicating robustness for this result.

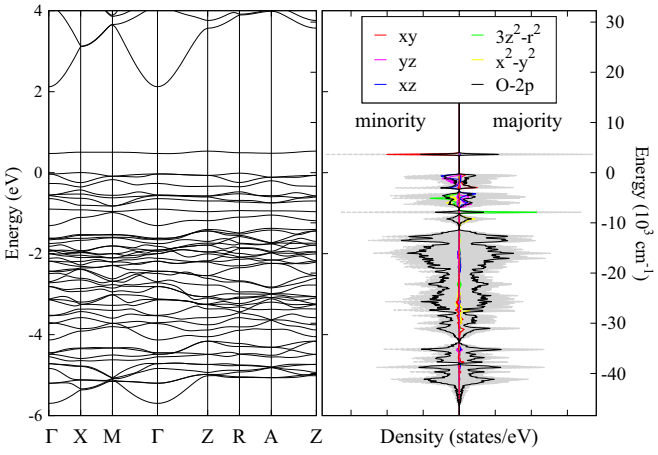

FIG. 4. Band structure (left) and density of states of $Ba_2CuGe_2O_7$ (right), with projection on majority and minority spin-polarized orbital states Cu-d and O-p. The Fermi level is set at the valence band maximum.

B. The electronic structure of $Ba_2CuGe_2O_7$

Figure 4 shows the calculated band structure (left), the total density of states (right) and its decomposition into Cu-d and O-p orbital states. Valence bands between −1.5 and −6 eV have predominantly O-p character, whereas valence and conduction bands between −1.5 and 0.6 eV show predominantly Cu-d character with a non-negligible admixture of O-p orbitals. The distorted tetrahedral coordinations of Cu ions is expected to affect the electronic structures due to crystal-field splitting effects, as in compounds with similar melilite structure [42,43]. For an ideal tetrahedral crystal field, the d levels of Cu are split in higher-energy threefold degenerate t_2 and lower-energy

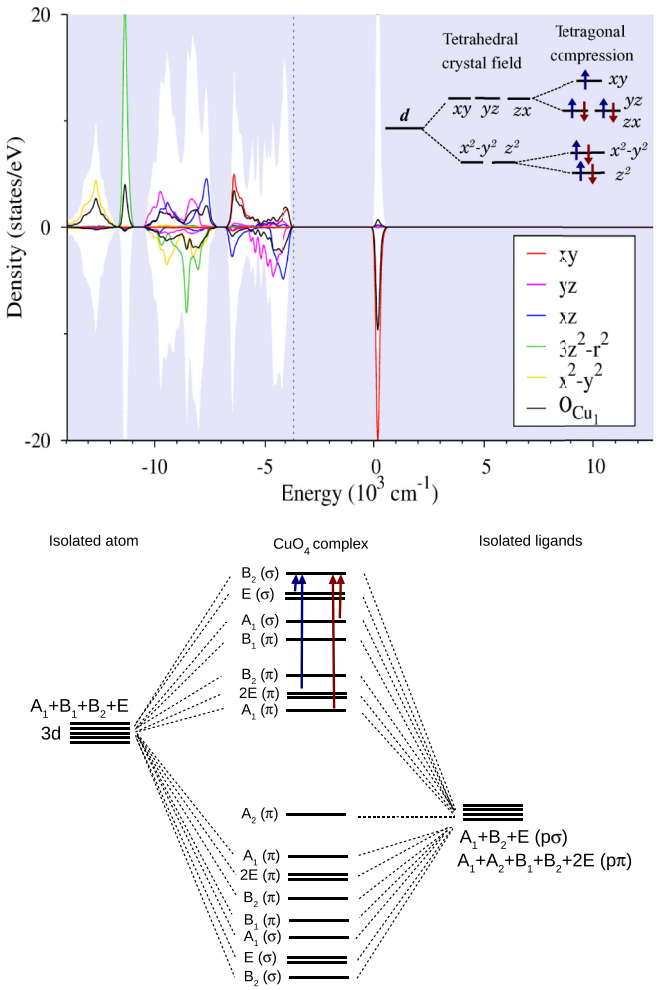

FIG. 5. Top: Zoomed view of the density of states projected onto the orbital d states of Cu1 and the p states of the surrounding oxygens forming the O_4 distorted tetrahedron. This picture confirms the crystal-field effects schematically shown in the inset and the strong pd hybridizations. Minority-spin states are symbolically associated with a negative density of states. The vertical dotted line represents the Fermi energy, while the energy reference on the x axis has been shifted to the lowest unoccupied peak to ease the comparison with optical spectra. Bottom: molecular-orbital diagram for a distorted CuO_4 tetrahedron with D_{2d} point-group symmetry. Vertical lines denote the (lowest-energy) symmetry-allowed dipole optical transitions for in-plane (blue arrows) and out-of-plane (red arrows) polarization of the radiation field.

twofold degenerate e levels, as schematically shown in the inset of Fig. 5(a). The c-axis compression is expected to further split the t_2 levels in lower-energy twofold levels with d_{yz},d_{zx} character and a higher-energy d_{xy} level. The compression is measured by the deviation of α,β from the ideal, undistorted value $\simeq 109.5^\circ$ and, as it increases, the level splitting is also expected to increase.

A deeper understanding of the electronic structure is provided by the analysis of the single-site electronic structure of a Cu atom in the distorted oxygen tetrahedron. The CuO_4 tetrahedra in BCGO belong to the D_{2d} point group, and accordingly the orbital states of an isolated Cu ion can be classified according to their irreducible representations as A_1, B_1, B_2, and E, corresponding to d_{z^2}, $d_{x^2-y^2}$, d_{xy}, and (d_{yz},d_{zx}) orbital states, respectively. Similarly, the molecular orbitals of the isolated ligands can be classified, on the basis of general symmetry analysis, as $\Gamma(p\sigma) = A_1 + B_2 + E$ (four states) and $\Gamma(p\pi) = A_1 + A_2 + B_1 + B_2 + 2E$ (eight states) for σ and π bonding, respectively. The resulting molecular-orbital diagram of the CuO_4 complex is depicted in Fig. 5(b), showing in fact that t_2 and e states of the undistorted tetrahedra are split in (b_2, e) and (a_1, b_1) states, respectively. As a consequence of the reduced symmetry of the distorted tetrahedron, several hybridization channels are allowed, which result in a strong mixing of Cu-d and O-p states. This indeed reflects into the projected density of states shown in Fig. 5(a), where the contribution of the four oxygens surrounding the selected Cu ion is shown alongside the d-states contributions. Such strong hybridization of d and p orbital states is expected to lead to dd optical transitions, at the same time suggesting a foreseeable dependence on local distortions. General symmetry arguments allow one to identify the possible optical dipole transitions for different field polarizations, which are shown as vertical arrows in Fig. 5(b).

C. Calculation of the optical conductivity in the *ab* plane and along the *c* axis

In order to compare the above results with the optical spectra in Sec. II, we have calculated the optical conductivity in the independent-particle approximation using the Kubo-Greenwood formula [44,45]

$$\sigma_{\alpha\beta}(\omega) = \frac{ie^2\hbar}{N_k\Omega_c}\sum_{\boldsymbol{k},n,m}\frac{f_{m\boldsymbol{k}}-f_{n\boldsymbol{k}}}{\varepsilon_{m\boldsymbol{k}}-\varepsilon_{n\boldsymbol{k}}}\frac{v^{nm}_{\alpha\boldsymbol{k}}\,v^{mn}_{\beta\boldsymbol{k}}}{\varepsilon_{m\boldsymbol{k}}-\varepsilon_{n\boldsymbol{k}}-(\hbar\omega+i\eta)}, \quad (1)$$

where e is the electron charge, Ω_c is the cell volume, and N_k is the number of k points used for the Brillouin-zone sampling. Indices α,β denote Cartesian directions, $\varepsilon_{n\boldsymbol{k}}$ is the Kohn-Sham energy at crystal momentum $\boldsymbol{k}$ with band index n, and $f_{n\boldsymbol{k}}$ is the Fermi-Dirac distribution function, while η is an adjustable smearing parameter. The matrix elements $v^{nm}_{\alpha\boldsymbol{k}} = \langle\psi_{n\boldsymbol{k}}|\hat{v_\alpha}|\psi_{m\boldsymbol{k}}\rangle$ of the full velocity operator $\hat{v}_\alpha = -i/\hbar[\hat{r}_\alpha, H]$ and the numerical integration of Eq. (1) have been evaluated using a Wannier interpolation scheme with adaptive broadening [46,47] as implemented in the Wannier90 code [48]. Bands in the energy window ranging from -6 eV to 0.6 eV have been projected onto Cu-d and O-p states. The Fermi level has been set to the value calculated from DFT, and a $70 \times 70 \times 70$ k-point mesh has been adopted for numerical integration. The real part of the calculated optical conductivity parallel and perpendicular to the ab plane is shown in Fig. 6, alongside with the joint density of states (JDOS):

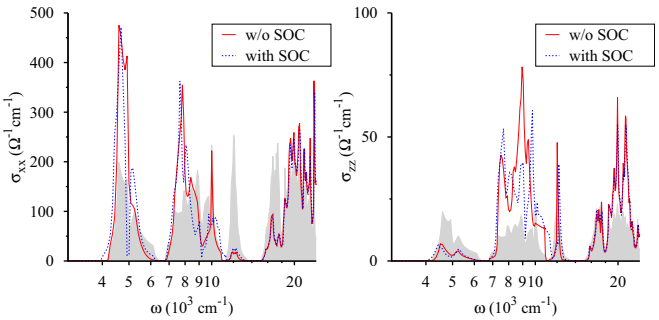

FIG. 6. Optical conductivity σ_{xx} (in plane, left) and σ_{zz} (out-of-plane, right) calculated for the optimized structure. The shaded area represents the joint density of states (JDOS), which has been multiplied by a factor of 10 in the left panel to ease the comparison. Dotted lines show the corresponding optical conductivities calculated with spin-orbit-coupling correction.

$$\rho(\omega) = \frac{1}{N_k}\sum_{\boldsymbol{k},n,m} f_{n\boldsymbol{k}}(1-f_{m\boldsymbol{k}})\delta(\varepsilon_{m\boldsymbol{k}}-\varepsilon_{n\boldsymbol{k}}-\hbar\omega). \quad (2)$$

The JDOS already shows features in the range between 4000 cm^{-1} and 12 000 cm^{-1}, suggesting the electronic origin of the observed absorption in the MIR range. In-plane conductivity σ_{xx} shows well defined peaks in the MIR region that can be ascribed mostly to dd transitions; specifically, the peak at the lowest edge of the spectrum arises from intrasite optical transitions from the occupied states with E character (d_{yz}, d_{zx}) to the lowest unoccupied state with B_2 character (d_{xy}), while features appearing in the range 7000–10 000 cm^{-1} should be ascribed to intersite optical transitions, as one can infer by comparing the electronic DOS in Fig. 5(a) with the calculated optical spectra [49]. In agreement with the local picture provided in Fig. 5(b), the optical transitions from occupied d_{z^2} and $d_{x^2-y^2}$ states (with symmetry A_1 and B_1, respectively) to unoccupied d_{xy} states are strongly suppressed for in-plane polarization of the radiation field.

As for the radiation polarized along the c axis, on one hand a strong suppression of the lowest-energy peak is predicted, reflecting the fact that optical dipole transitions from E to B_2 should not be allowed in this setting. On the other hand, a well-defined peak at $\sim$11 000 cm^{-1} (corresponding to intersite A_1-B_2 transitions) is clearly observed, while the features in the range 7000–10000 cm^{-1} should arise from intrasite absorption. For both polarizations, features appearing at frequencies larger than 12 000 cm^{-1} should be ascribed to pd transitions. Despite the calculated spectra are consistent with the ones expected from the previous symmetry-based analysis, we found a significant difference between the absolute values of σ_{xx} and σ_{zz}, which is not confirmed by the experimental results, albeit being compatible with the layered structure of BCGO. The origin of such discrepancy might be related to the approximations made in our numerical simulations, which may not fully capture (local) correlation effects.

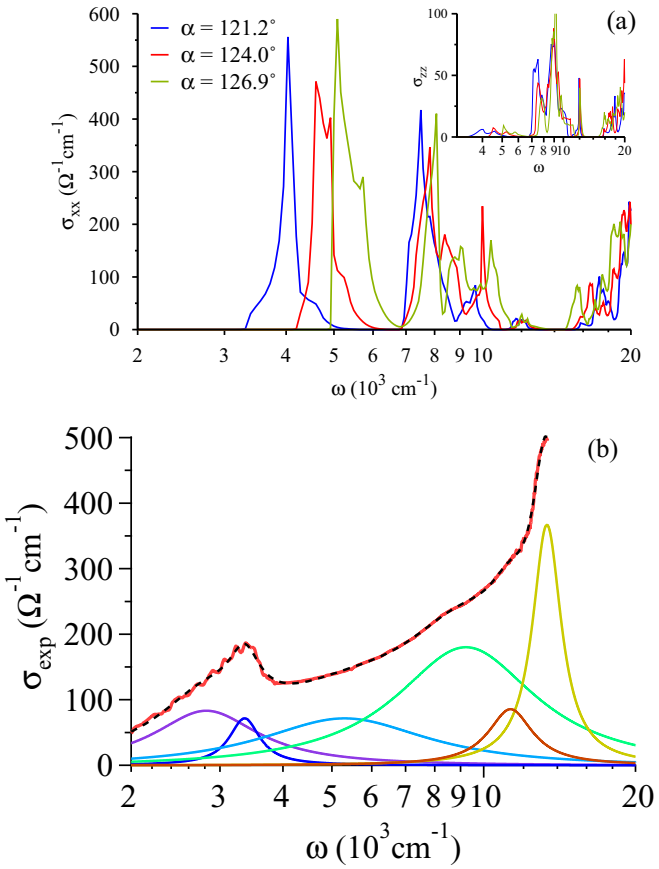

FIG. 7. (a) In-plane σ_{xx} (inset: out-of-plane σ_{zz}) optical conductivity of the optimized structure evaluated for three values of the angle α parametrizing distortion respect to the ideal CuO_4 tetrahedron ($\alpha \simeq 109.5^\circ$); (b) decomposition of the experimental, ab-plane $\sigma(\omega)$ in Fig. 2(a) at 20 K in terms of a sum of Lorentzians, for an easier comparison with the theoretical σ_{xx} in (a). The dashed line is the fitting curve to data (solid red line).

Finally, small modifications of the optical spectra are observed when spin-orbit coupling is included in the calculations, most notably in the frequency range associated with dd transitions. Such SOC-induced splittings do not affect the gross features discussed above, at the same time being too tiny to be experimentally observed.

It is expected that the strong sensitivity of the E (d_{yz}, d_{zx}) -B_2 (xy) splitting to the tetragonal compression [see inset of Fig. 5(a)] leads to a sensitivity of the optical properties, not only for the position of the bands, but also for the spectral weight which will be affected by pd hybridization. Therefore, we calculated the optical conductivity for three structures with different degrees of tetrahedral distortions, where the angles α,β have been changed while keeping fixed the cell volume and the bond lengths; the results are shown in Fig. 7(a). Interestingly, the most meaningful changes can be seen in the lowest-frequency peak and in the high-frequency edge around 13 000 cm^{-1}, while features at intermediate frequency are less affected, even though an overall hardening of all dd transitions is always found when increasing the local distortions.

IV. COMPARISON WITH THE EXPERIMENT

Figure 7(b) shows a fit to the experimental $\sigma(\omega)$ of the ab plane in Fig. 2 at 20 K, in terms of a sum of Lorentzians. As one can see, there is a qualitative but meaningful agreement with the theoretical σ_{xx} in (a), especially if one considers the virtual absence of broadening in the latter quantity. In the experimental curve in (b), the three peaks between 3000 and 5000 cm^{-1} (violet and blue lines) can be compared with the structured band in (a) predicted between 3500 and 5000 cm^{-1} (the best agreement being obtained for the smallest tetrahedral distortion, blue lines); the broad and well evident band peaked at 9000 cm^{-1} (green line) may account for the group of lines in (a) between 7000 and 11 000 cm^{-1}; finally, the two peaks in (b) at $\omega > 10\,000$ cm^{-1} build up the optical gap which appears in (a) at similar frequencies as the edge of a band which, in Fig. 6 extends to the whole visible range.

The optical conductivity predicted for the c axis [see Fig. 6, right panel, and inset of Fig. 7(a)] is significantly smaller than both the $\sigma(\omega)$ calculated for the ab plane and that measured along the c axis [see Fig. 2(b)]. The origin of such discrepancy is probably rooted on the theoretical methodology which cannot deal adequately with the strong Mott localization effects present in the system [34]. One should keep in mind that for $Ba_2CuGe_2O_7$ the ratio of the Hubbard U energy to the bandwidth is expected to be much larger than, for example, in the parent compounds of high-T_c cuprates. Indeed, in BCGO the magnetic ordering temperature $T_C \sim 3$ K so that the superexchange energy $J \propto t^2/U$ (where t is the hopping rate, proportional to the bandwidth) is on the order of 1 meV compared to 100 meV in cuprates. Since U should be roughly the same, we estimate the ratio U/t to be ten times larger than in high-T_c cuprates. Under these conditions, Mott localization effects are expected to be dominant, especially along the c axis of the layered structure, explaining the problems encountered by the computation. In this strong-correlation regime, also excitonic effects are expected to be important and were not taken into account. Taking these problems together, we find the amount of disagreement between theory and experiment to be surprisingly mild.

Having established the correspondence between the theoretical and experimental electronic bands, let us now discuss the second main result reported here, namely their temperature dependence. Figure 7(a) shows that the mid-IR peak is substantially shifted toward higher energies as the CuO_4 tetrahedra are more distorted, while the high-frequency peak shows an opposite shift. These findings can be rationalized in terms of (distorted) tetragonal crystal-field and pd hybridization which produces the B_2-E splitting and lowers the symmetry of the wave functions. Therefore, a meaningful agreement with the rather surprising result of the experiment is obtained under the single assumption that, in BCGO, the Cu-O tetrahedra are increasingly distorted when lowering the temperature. This prediction should be confirmed by temperature-dependent diffraction measurements, presently not available to our knowledge. Nevertheless, a previous investigation of the BaCuGeO vibrational dynamics indicates that a few phonons, like the infrared-active mode 4 of the c axis [21] and the Raman mode 21 [22] exhibit a remarkable hardening at low temperature. They are both bending modes of the Cu-O bonds

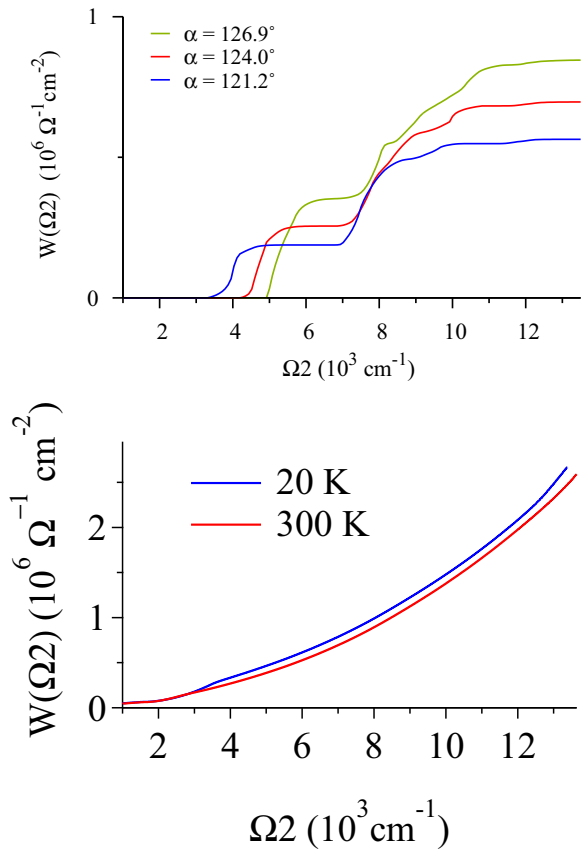

FIG. 8. Calculated (top) and measured (bottom) optical spectral weight for the *ab* plane of $Ba_2CuGe_2O_7$ at 20 K and 300 K for Ω2 spanning the mid and near infrared. Under our assumptions, the larger distortion corresponds to the lowest temperature.

within the CuO_4 tetrahedra (see Supplemental Material to Ref. [21] and Fig. 5 of Ref. [22], respectively), which can be highly sensitive to low-temperature changes of the α angle through the anharmonic terms of the interatomic potential.

Since the lowest-energy peak is strongly suppressed for field polarization along c, the effect is less visible for the calculated σ_{zz}, in qualitative agreement with experimental MIR band where no appreciable shift is observed; on the other hand, the high-energy features still shift toward lower energies as the local distortions increase.

For sake of completeness we have also calculated the optical spectral weight

$$W(T) = \int_{\Omega 1}^{\Omega 2} \sigma(\omega, T) d\omega \qquad (3)$$

in the *ab* plane at 20 K and 300 K for $\Omega 1 = 70\ \mathrm{cm}^{-1}$ and Ω2 varying up to 13 000 cm^{-1}. We have used, for the phonon region, data reported in Ref. [21], and the $\sigma(\omega)$ of Fig. 2 for $\omega > 700\ \mathrm{cm}^{-1}$. We notice that the curves for different temperatures [Fig. 8(b)] do not converge within the energy range of the experiment. In order to fulfill the f sum rule [50], such convergence should then occur in the visible or UV range, as it often occurs in strongly correlated systems [33] as $Ba_2CuGe_2O_7$ certainly is. Finally, W has been also calculated for the theoretical $\sigma(\omega)$, and reported in Fig. 8(a). A comparison with panel (b) shows that the calculations are successful in explaining both the total oscillator strength of the bands, within a factor of ∼2, and its average slope vs Ω2. The "steps" appearing in Fig. 8(a) are smeared out in the experiment by strong broadening effects.

V. CONCLUSIONS

In conclusion, the present work completes our optical study of the Dzyaloshinsky-Moriya multiferroic $Ba_2CuGe_2O_7$, initiated with an infrared and Raman investigation of its lattice dynamics, by measuring the optical conductivity of BCGO in the region of its electronic bands, both in the *ab* plane and along the *c* axis. Three groups of absorption bands, partially superimposed, have been identified, in the midinfrared, near infrared, and visible range. The band structure has then been theoretically determined by a DFT approach and the resulting optical conductivity has been calculated by the Kubo-Greenwood formula. Also the resulting, theoretical $\sigma(\omega)$ exhibits three groups of bands, whose frequencies are in substantial agreement with the observations. The features appearing in the frequency range 3000–12000 cm^{-1} can be ascribed mostly to *dd* transitions, while those at higher frequencies have a pronounced O-*p* character. Inclusion of the spin-orbit coupling correction has been shown to produce minor effects.

Even if the use of conventional DFT has required ad hoc assumptions to describe the BCGO electronic structure, like the introduction of a broken symmetry state to obtain an insulating phase, we recall that such an approach is often used in the literature and here is specially suited. Indeed, as the coupling between CuO_4 tetrahedra is very weak, one expects that intersite transitions will also be weak. The optical conductivity will then be dominated by electronic transitions within single tetrahedra and therefore it will be poorly sensitive to an artificial magnetic ordering among different tetrahedra.

The experiment also shows that, interestingly, both the MIR band of the *ab* plane and those for both polarizations in the visible range, are strongly temperature dependent. However, while the MIR band hardens from 300 K to 20 K by about 1000 cm^{-1}, the latter ones—which provide a sort of optical gap around 13 000 cm^{-1} at room temperature—surprisingly soften by more than 1000 cm^{-1} when cooling the sample. This behavior is opposite to that encountered, for example, in cuprates, where the Cu-O charge-transfer band hardens when, for $T \to 0$, the lattice contraction compresses the Cu-O bonds. As a result, the curves of the experimental spectral weight W at 20 and 300 K never converge up to the visible range, suggesting that the f sum rule is fulfilled at higher energy as often encountered in strongly correlated systems.

Even if our DFT calculations cannot provide T-dependent results, we have investigated the possibility that the observed effects are due to a distortion of the Cu-O bond angles in the CuO_4 tetrahedra. We have indeed found that both the calculated MIR band and the edge of the band in the visible are extremely sensitive to those parameters and that their opposite shifts can be qualitatively reproduced by variations in the Cu-O bond angle $\alpha = O_{up}$-Cu-O_{up} by less than 3°. Also the calculated spectral weight W, whose frequency dependence and absolute value are not far from the observed values, is consistent with the assumption of a stronger distortion at

low temperature. We are then led to suppose that the main effect of temperature on the BCGO lattice is such distortion, as also indicated by the temperature dependence previously observed in some vibrations of the Cu-O tetrahedra. In this respect, it would be interesting to investigate the pressure dependence of the optical properties of $Ba_2CuGe_2O_7$, which would allow one to verify directly the role of local distortions of CuO_4 in determining the electronic band structure and optical conductivity of this class of Dzyaloshinsky-Moriya materials. As a further development, the potential impact of such distortions on the magnetoelectric properties of this noncentrosymmetric material, whose origin has been ascribed to a substantially local *p-d* hybridization mechanism, could be investigated from both a theoretical and an experimental point of view.

ACKNOWLEDGMENTS

We wish to thank S. Picozzi for helpful discussions. This work has been partially funded by a PRIN project of the Italian Ministero dell'Istruzione, dell'Università e della Ricerca.

[1] N. A. Spaldin and M. Fiebig, Science **309**, 391 (2005), and references therein.
[2] M. Tanaka, K. Siratori, and N. Kimizuka, J. Phys. Soc. Jpn. **53**, 760 (1984).
[3] N. Ikeda, H. Ohsumi, K. Ohwada, K. Ishii, T. Inami, K. Kakurai, Y. Murakami, K. Yoshii, S. Mori, Y. Horibe, and H. Kito, Nature (London) **436**, 1136 (2005).
[4] I. Dzyaloshinskii, J. Phys. Chem. Solids **4**, 241 (1958).
[5] T. Moriya, Phys. Rev. **120**, 91 (1960).
[6] W. Eerenstein, N. D. Mathur, and J. F. Scott, Nature (London) **442**, 759 (2006), and references therein.
[7] U. Nagel, R. S. Fishman, T. Katuwal, H. Engelkamp, D. Talbayev, H. T. Yi, S.-W. Cheong, and T. Rõõm, Phys. Rev. Lett. **110**, 257201 (2013).
[8] R. S. Fishman, J. T. Haraldsen, N. Furukawa, and S. Miyahara, Phys. Rev. B **87**, 134416 (2013).
[9] A. Zheludev, G. Shirane, Y. Sasago, N. Koide, and K. Uchinokura, Phys. Rev. B **54**, 15163 (1996); A. Zheludev, S. Maslov, G. Shirane, I. Tsukada, T. Masuda, K. Uchinokura, I. Zaliznyak, R. Erwin, and L. P. Regnault, *ibid.* **59**, 11432 (1999).
[10] I. Tsukada, J. Takeya, T. Masuda, and K. Uchinokura, Phys. Rev. B **62**, R6061(R) (2000).
[11] J. Chovan, M. Marder, and N. Papanicolaou, Phys. Rev. B **88**, 064421 (2013).
[12] H. Murakawa, Y. Onose, and Y. Tokura, Phys. Rev. Lett. **103**, 147201 (2009).
[13] H. Murakawa, Y. Onose, S. Miyahara, N. Furukawa, and Y. Tokura, Phys. Rev. Lett. **105**, 137202 (2010).
[14] H. Murakawa, Y. Onose, S. Miyahara, N. Furukawa, and Y. Tokura, Phys. Rev. B **85**, 174106 (2012).
[15] T. Masuda, S. Kitaoka, S. Takamizawa, N. Metoki, K. Kaneko, K. C. Rule, K. Kiefer, H. Manaka, and H. Nojiri, Phys. Rev. B **81**, 100402(R) (2010).
[16] A. Zheludev, T. Sato, T. Masuda, K. Uchinokura, G. Shirane, and B. Roessli, Phys. Rev. B **68**, 024428 (2003).
[17] M. Soda, S. Hayashida, B. Roessli, M. Månsson, J. S. White, M. Matsumoto, R. Shiina, and T. Masuda, Phys. Rev. B **94**, 094418 (2016).
[18] Thuc T. Mai, C. Svoboda, M. T. Warren, T.-H. Jang, J. Brangham, Y. H. Jeong, S.-W. Cheong, and R. Valdés Aguilar, Phys. Rev. B **94**, 224416 (2016).
[19] V. Hutanu, A. Sazonov, M. Meven, H. Murakawa, Y. Tokura, S. Bordács, I. Kézsmárki, and B. Náfrádi, Phys. Rev. B **86**, 104401 (2012).
[20] I. Kézsmárski, N. Kida, H. Murakawa, S. Bordács, Y. Onose, and Y. Tokura, Phys. Rev. Lett. **106**, 057403 (2011).
[21] A. Nucara, W. S. Mohamed, L. Baldassarre, S. Koval, J. Lorenzana, R. Fittipaldi, G. Balakrishnan, A. Vecchione, and P. Calvani, Phys. Rev. B **90**, 014304 (2014).
[22] F. Capitani, S. Koval, R. Fittipaldi, S. Caramazza, E. Paris, W. S. Mohamed, J. Lorenzana, A. Nucara, L. Rocco, A. Vecchione, P. Postorino, and P. Calvani, Phys. Rev. B **91**, 214308 (2015).
[23] R. Fittipaldi, L. Rocco, M. Ciomaga Hatnean, V. Granata, M. R. Lees, G. Balakrishnan, and A. Vecchione, J. Cryst. Growth **404**, 223 (2014).
[24] F. Wooten, *Optical Properties of Solids* (Academic Press, New York, 1972), p. 249.
[25] J. Bhosale, A. K. Ramdas, A. Burger, A. Muñoz, A. H. Romero, M. Cardona, R. Lauck, and R. K. Kremer, Phys. Rev. B **86**, 195208 (2012).
[26] Y. Tokura, K. Kikuchi, T. Arima, and S. Uchida, Phys. Rev. B **45**, 7580 (1992).
[27] S. Lupi, M. Ortolani, and P. Calvani, Phys. Rev. B **69**, 180506(R) (2004).
[28] G. Kresse and D. Joubert, Phys. Rev. B **59**, 1758 (1999).
[29] J. P. Perdew, A. Ruzsinszky, G. I. Csonka, O. A. Vydrov, G. E. Scuseria, L. A. Constantin, X. Zhou, and K. Burke, Phys. Rev. Lett. **100**, 136406 (2008).
[30] J. P. Perdew, A. Ruzsinskky, L. A. Constantin, J. Sun, and G. I. Csonka, J. Chem. Theory Comput. **5**, 902 (2009).
[31] F. G. Eich, S. Pittalis, and G. Vignale, Phys. Rev. B **88**, 245102 (2013).
[32] W. Kohn, A. Savin, and C. A. Ullrich, Int. J. Quantum Chem. **100**, 20 (2004).
[33] H. Eskes, A. M. Oleś, M. B. J. Meinders, and W. Stephan, Phys. Rev. B **50**, 17980 (1994).
[34] Z.-J. Ying, V. Brosco, G. M. Lopez, D. Varsano, P. Gori-Giorgi, and J. Lorenzana, Phys. Rev. B **94**, 075154 (2016).
[35] J. A. S. Oliveira, *Crystal-chemical investigations in the systems* CuO-BaO-SiO_2-GeO_2 and BaO-Rh_2O_3, Heidelberger geowissenschaftliche Abhandlungen (U. Thesis), 1993, http://hdl.handle.net/10068/131783.
[36] M. Tovar, R. E. Dinnebier, and W. Eysel, *The* Cu(II)O_4 *Tetrahedron in the Åkermanite Structure*, Proc. 5th European Powder Diffraction Conference, Parma (1997); Mater. Sci. Forum **278**, 750 (1998).
[37] F. Tran, J. Stelzl, and P. Blaha, J. Chem. Phys. **144**, 204120 (2016).

[38] Z. Wu and R. E. Cohen, Phys. Rev. B **73**, 235116 (2006).
[39] L. A. Constantin, A. Terentjevs, F. Della Sala, P. Cortona, and E. Fabiano, Phys. Rev. B **93**, 045126 (2016).
[40] J. P. Perdew, K. Burke, and M. Ernzerhof, Phys. Rev. Lett. **77**, 3865 (1996).
[41] S. L. Dudarev, G. A. Botton, S. Y. Savrasov, C. J. Humphreys, and A. P. Sutton, Phys. Rev. B **57**, 1505 (1998).
[42] K. Yamauchi, P. Barone, and S. Picozzi, Phys. Rev. B **84**, 165137 (2011).
[43] P. Barone, K. Yamauchi, and S. Picozzi, Phys. Rev. B **92**, 014116 (2015).
[44] R. Kubo, J. Phys. Soc. Jpn. **12**, 570 (1957).
[45] D. A. Greenwood, Proc. Phys. Soc. (London) **A71**, 585 (1958).
[46] X. Wang, J. R. Yates, I. Souza, and D. Vanderbilt, Phys. Rev. B **74**, 195118 (2006).
[47] J. R. Yates, X. Wang, D. Vanderbilt, and I. Souza, Phys. Rev. B **75**, 195121 (2007).
[48] A. Mostofi, J. R. Yates, Y.-S. Lee, I. Souza, D. Vanderbilt, and N. Marzari, Comput. Phys. Commun. **178**, 685 (2008).
[49] Notice that, due to the C-type antiferromagnetic configuration, minority spins on the Cu2 ion are parallel to majority spins on Cu1 and vice versa.
[50] M. Dressel and G. Grüner, *Electrodynamics of Solids* (Cambridge Univ. Press, Cambridge, UK, 2002).